


Modes and Progression of Tool Deterioration and Their Effects on Cutting Force during End Milling of 718Plus Ni-Based Superalloy using Cemented WC-Co Tools

Nurul Hidayah Razak

A thesis submitted to Auckland University of Technology in fulfilment of the
requirements for the degree of Doctor of Philosophy

2017

School of Engineering, Computer and Mathematical Sciences

PERPUSTAKAAN  UNIVERSITI MALAYSIA PAHANG	
No. Perolehan 119313	No. Panggilan TJ 1191 H53 2017 Thesis
Tarikh 11 AUG 2017	

ABSTRACT

Understanding the detailed progression of cutting tool deterioration and how deterioration affects cutting force (F) during milling of difficult-to-cut Ni-based superalloys is important for the improvement of machinability of the alloys. It also serves to clarify whether and how an F -based method for monitoring tool deterioration is possible. This understanding is however far from sufficient, as is explained in this thesis after a comprehensive review of the literature. The aim of the present research is thus to determine and explain the modes and progression of tool deterioration and how cutting forces may vary due to the various deterioration features of the cutting tool edge.

Experimentally, the study started by using a typical milling condition with both uncoated and coated cemented carbide (WC-Co) tools. Milling was conducted in either dry or wet conditions. After each pass of a selected distance, the tool was examined in detail in the same manner. Thus, tool deterioration could be monitored more closely and failure mechanisms could be identified and explained. Following on the study on determining the modes of tool deterioration, the progress of deterioration and cutting forces during milling were carefully monitored. Through analysing the monitored tool deterioration features and measured force data, how edge wear, chipping and breakage in cutting edge and beyond the edge contribute to the variation of cutting forces could be studied and better understood. Furthermore, experiments have also been conducted using workpiece in a hardened state.

It has been observed that the commonly recognised build-up layer in the initial stage does not significantly affect the tool deterioration process. Instead, from the beginning of milling, cutting forces/stresses could cause small chipping locally in the initially sharp cutting edge. Fracturing locally with cracks propagating outside the cutting edge along the flank face in the subsurface region could also take place and was consistent with the direction of the cutting force. There was an initial period of time during which a number of microcracks had initiated in and near the cutting edge on the rake face side. These cracks soon propagated resulting in extensively fracturing and blunting of the tool. Coating of the tools had provided little protection as in the cutting edge area the coating had broken away soon after milling started. The major tool failure mode was Co binder material having heavily deformed to fracture, separating the WC grains. Loss of strength in binder material at cutting temperatures

is also discussed. As would be expected, the general trend of how F increased as the number of pass (N_{pass}) increased agreed with the general trend of increasing flank wear (VB) as N_{pass} increased. However, the F - VB_{max} plot has shown a rather poor F - VB_{max} relationship. This was the result of the different modes of tool deterioration affecting VB_{max} differently, but VB_{max} did not represent fully the true cutting edge of the deteriorating tool insert. Chipping and breakage of the inserts confined in the cutting area, resulting in the significant blunting of the edge area, causing a high rate of F increase as VB_{max} increased and completely deteriorated 6 minutes within of milling time. Fracturing along the face of thin pieces effectively increased VB_{max} without increasing the cutting edge area and without further blunting the edge, thus no increase in F was required. The high rate, meaning high $\Delta F/\Delta VB_{max}$, results from the effect of the edge deterioration/blunting on the reducing the effective rake angle and thus increasing F is suggested and discussed. The use of coolant has not been found to affect tool deterioration/life and cutting force. Explanation for this will be given considering the deformation zone for which coolant does not have an effect. An increase in feed rate has reduced the tool life and the mode of deterioration has become more edge chipping/fracturing dominant, leading to a better F - VB_{max} relationship.

Finally, it has been observed that the rate of tool deterioration is not higher when the hardened workpiece material is used. The modes and progression of deterioration of tools using hardened workpiece were determined to be comparable to those when annealed workpiece was used. Furthermore, the trends of increase in cutting force as milling pass increases have been observed to be similar for both workpiece material conditions. Interrupt milling experiments followed by hardness mapping has indicted that the workpiece hardened state has not affected the deformation area significantly, although increase in hardness in a similar amount in the severe deformed region has been found for both cases. It is suggested that temperature increases in the narrow deformation zone to be similar for both workpiece conditions and at high temperatures hardening mechanisms do not operate, and thus cutting force values do not differ significantly. Furthermore, the modes and rate of tool deterioration on the hardened workpiece was comparable to the annealed workpiece.

ACKNOWLEDGEMENTS

I would like to acknowledge and extend my heartfelt gratitude to my primary supervisor, Prof Zhan Chen for the continuous support of my Ph.D study and related research, for his patience, motivation, and immense knowledge. His guidance helped me in all the time of research and writing of this thesis. I could not have imagined having a better advisor and mentor for my Ph.D study. I also would also like to thank my secondary supervisor, AP Timotius Pasang for his continuous support guiding me through the thesis writing process by giving me his best effort.

My sincere thanks also goes to Jim Crossen, Ross Jamieson, Mark Masterston, Tim Luton, Thomas Jones and Patrick Connor for their hard work, expertise and patience. Without their precious support, it would not be possible to conduct this research.

My appreciation also extends to Karl Davidson for stimulating discussion and for the sleepless nights we were working together before the deadline. I also would like to thank Doddy, Evtaleny, and Yuan and other research group members for all the fun we have had in the last three years. I also thank my dearest friends Hemyza Budin, Har Einur Azrin, Nurul Syuhada Mohamed, Ili Ayuni Johan and Ridhuan Abd. Rahim for providing support and friendship.

Most importantly, I would like to thank The Davidsons and Wendy Millen for their great support and unconditional love during difficult times. I would not have made it this far without them. Last but not least, I would like to thank my family especially my mother, Wan Rasnah Wan Idris, who have guided me throughout my life. She has always sacrificed her time and has continuously supported me in achieving my dreams and goals. I would like to thank her for all her love, support and encouragement for me. I specially dedicate this work to my beloved late father, Razak Latif and I wish he could smile for me.

LIST OF PUBLICATIONS

The following papers have been published over the course of this research.

Journal papers:

Razak, NH, Chen, ZW and Pasang, T, Modes of Tool Deterioration during Milling of 718Plus Superalloy Using Cemented Tungsten Carbide Tools, *Wear* 316 (2014): 92-100.

Razak, NH, Chen, ZW and Pasang, T, Progression of Tool Deterioration and Related Cutting Force during Milling of 718Plus Superalloy using Cemented Tungsten Carbide Tools, *International Journal Advance Manufacturing Technology* (2016) 86: 3203-3216.

Conference paper:

Razak, NH, Chen, ZW and Pasang, T, Relationship Between Tool Deterioration and Cutting force during Milling of a Nickel-Based Superalloy Using Cemented Carbide Tool, *Proceeding of the ASME 2015 International Mechanical Engineering Congress and Exposition (IMECE2015)*, November 13-19, 2015, Houston, Texas.

TABLE OF CONTENTS

ABSTRACT	ii
ACKNOWLEDGEMENTS	iv
LIST OF PUBLICATIONS	v
TABLE OF CONTENTS	vi
LIST OF FIGURES	viii
LIST OF TABLES	xviii
NOMENCLATURE.....	xix
ATTESTATION OF AUTHORSHIP	xxi
Chapter 1: Introduction and Literature Review	1
1.1 Background of the Study.....	1
1.2 An Introduction on Tool Deterioration.....	3
1.3 Current Assessment Methods on Tool Deterioration	7
1.4 Tool Wear Mechanisms.....	10
1.5 Current Understanding on Gradual Wear.....	10
1.6 The Other Modes of Tool Deterioration.....	20
1.7 Model Relating Tool Deterioration to Milling Time or Distance	24
1.8 Effect of Cooling on Tool Deterioration	26
1.9 Effect of Tool Coating on Tool Deterioration.....	29
1.10 Effect of Workpiece Hardened State on Tool Deterioration	32
1.11 Effect of Tool Deterioration on Cutting Force.....	33
1.12 The Scope of This Study	36
Chapter 2: Experimental Design and Procedures.....	38
2.1 Milling Machine and Clamping system	38
2.2 Workpiece and Cutting Tools Materials.....	40
2.3 Workpiece Hardness and Strength Measurements	43
2.4 Milling Parameters and Conditions.....	45
2.5 Dynamometer and Force monitoring.....	48

2.6	Sample Preparation and Examination	50
2.7	Tool Deterioration Monitoring.....	52
Chapter 3: Modes of Tool Deterioration.....		56
3.1	Flank Deterioration – Early Stage	56
3.2	Flank Deterioration – Growth Stage.....	60
3.3	Deterioration Observed on All Three Faces.....	61
3.4	Deterioration of Coated Tools	65
3.5	Further Discussion on Modes and Measures of Tool Deterioration.....	67
3.6	Mode of Fracture	69
3.7	Summary	70
Chapter 4: Cutting Force and Progression of Tool Deterioration.....		71
4.1	Features of Forces During Milling	71
4.2	Examination on the Effect of Coating on Cutting Force.....	77
4.3	Effect of Tool Deterioration on Cutting Force.....	80
4.4	Further Discussion on Cutting Force Relating to Deterioration of Cutting Edge .	88
4.5	Examination on Cutting Edge Condition Affecting Deformation Zone	90
4.6	Effect of High Feed Rate on Cutting Force.....	94
4.7	Summary	103
Chapter 5: Tool Deterioration Influenced by Workpiece Heat Treatment State		104
5.1	Cutting Edge Deterioration	104
5.2	Trend of Cutting Force Increase Verse Milling Pass	115
5.3	Cutting Edge Condition Affecting Deformation Zone.....	121
5.4	Summary Plots on The Effect of Heat Treatment State	123
5.5	Overall Plots of Flank Wear and Cutting Force	125
Chapter 6: Conclusion.....		127
References		129

LIST OF FIGURES

Figure 1-1 Illustration of resultant force (F_R) and friction force (F_f) as the interaction between workpiece and cutting tool.....	1
Figure 1-2 Scanning Electron Microscope images (SEM) on tool failure of an uncoated cemented carbide tool; (a) side flank face and (b) rake face.....	3
Figure 1-3 Illustration of down-milling operation with image of tool holder and insert.....	4
Figure 1-4 Cutting edge view with (a) cutting edge (wear), (b) edge chipping and (c) heavy chipping, the primary deterioration modes further proposed in this study	5
Figure 1-5 Enlarged view near the cutting edge locations with cutting force and edge shear stress indicated	5
Figure 1-6 Standard wear nomenclature, (a) tool cutter, (b) illustration of VB assessment ..	7
Figure 1-7 Graph of flank wear, VB (mm) versus cutting time (min) [11].....	8
Figure 1-8 Illustration to indicate the true dimensional deterioration distances in a cross section	8
Figure 1-9 Measurement of tool wear. The original profile of the tool edge is shown as the discontinuous line [9].....	11
Figure 1-10 (a) Flank wear of an insert after six passes of down milling ($v_c = 30$ m/min, $f = 0.03$ mm/rev, $DOC = 1.2$ mm, $a_e = 2$ mm) from Li et al. [22] and (b) Illustration of VB assessment from various publications and true assessment of tool deterioration	12
Figure 1-11 Flank wear of TiAlN/AlCrN insert [11].....	13
Figure 1-12 Flank wear of a carbide tool at cutting speed, (V)=113.1m/min and feed rate, (f) = 0.05m/tooth [3].....	13
Figure 1-13 Maximum flank wear width and maximum chipped edge with on a cutter flute [4]	14
Figure 1-14 Illustration of cutting edge, flank face and rake face	14
Figure 1-15 Mapping of speculative wear causes, types and consequences, given by Zhu et al. [12] (there is a serious uncertainty in Zhu et al.'s quoting in regard to the sources of the map).....	16
Figure 1-16 (a) Images of the adhesion mechanism during the adhesion of workpiece material to tool, Illustration indicated the adhesive mechanism based on suggested opinion by Zhu et	

al. [12], (b) after taking off the tool material and (c) illustration the bonding strength BUL ($\sigma_{BUL} / \sigma_{WC-Co}$) and interface between the WC-Co ($\sigma_{int} / \sigma_{WC-Co}$)	17
Figure 1-17 Example of tool failure due to (a) abrasive mechanism, and (b) adhesion mechanism [12]	18
Figure 1-18 SEM images of the cutting corner location (top: rake face, left: side flank face and right: bottom flank face) of tools after end milling cutting ($v_c = 100$ m/min, $f = 0.15$ mm/rev and $DoC = 1.0$ mm) by Kadirgama et al.[5], (a) PVD TiAlN coated WC-Co tool after 180 mm milling (b) CVD TiN/TiCN/Al ₂ O ₃ coated WC-Co tool after 742 mm milling and (c) Illustration to aid the attachment and notch (s) location.....	21
Figure 1-19 SEM images of tool inserts: (a) an insert in an initial stage with rake face and flank face as indicated and clearly without a notch, (b) a down view on the rake face after notching (we have observed, outlined/labelled in white although authors have not) during ball-nose end milling by Kasim et al. [11]. Tool inserts were TiAlN/AlCrN coated (cutting conditions were not specified by authors) and (c) Illustration from Figure 1-19a, chipping at flank face (we identified)	22
Figure 1-20 Photos of a coated tool insert after: (a) 22.1 min, (b) 24.1 min, (c) 27.5 min, (d) 29.5, (e) 35.5 min and (f) 42.9 min under cutting condition of ($v_c = 50$ m/min, $f = 0.1$ mm/rev and axial depth of cut = 0.5, $a_e = 1.0$ mm) via dry condition. Top: rake face, left: bottom flank face and right: side flank face, scale on the photo is our approximation based on value of axial depth of cut [8].....	22
Figure 1-21 Photos of a coated tool insert after: (a) 20.8 min, (b) 28.8 min, (c) 44.9 min, (d) 57.0 min, 64.3 min and (f) 72.4 min under cutting condition of ($v_c = 50$ m/min, $f = 0.1$ mm/rev and axial depth of cut = 0.5, $a_e = 1.0$ mm) via MQL . Top: rake face, left: bottom flank face and right: side flank face, scale on the photo is our approximation based on value of axial depth of cut [8]	23
Figure 1-22 Scanning electron microscope (SEM) micrograph showing tool fracturing... 24	
Figure 1-23 Change in corner wear with cutting length for MQL machining with the ordinary nozzle. Cutting conditions: cutting speed, 1.3 m/s (78 m/min); depth of cut, 0.11 mm; feed rate, 0.1 mm/rev [29].....	26
Figure 1-24 Tool lives of three coated tools in MQL, wet and dry cutting, Cutting conditions: cutting speed, 1.0 m/s; feed rate, 0.1 mm/rev; depth of cut, 0.1mm; air pressure of MQL, 0.40MPa; Oil consumption of MQL, 16.8 ml/h [30]	27
Figure 1-25 Tool wear VB with cutting time under different cutting conditions [8]	27
Figure 1-26 Evolution of tool life in dry, oil based emulsion, cold air and cryogenic turning of Inconel 718 [48].....	28

Figure 1-27 Notch wear progression under different cooling conditions [34].....	28
Figure 1-28 Development of average flank wear when face milling Inconel 718 and feed rate of 0.08 mm per tooth [17]	29
Figure 1-29 Tool wear plot in terms of length cut [36]	30
Figure 1-30 Performance of TiAlN-multilayer variants in turning Inconel 718 [37]	30
Figure 1-31 Tool lives of three coated tools in MQL, wet and dry cutting, Cutting conditions: cutting speed, 1.0 m/s; feed rate, 0.1 mm/rev; depth of cut, 0.1mm; air pressure of MQL, 0.40MPa; Oil consumption of MQL, 16.8 ml/h [30]	31
Figure 1-32 Box plots, whisker and outliers of tool life with different cutting tool coatings [40]	32
Figure 1-33 Illustration of resulted force (F_R) and friction force (F_f) as the interaction between workpiece and cutting tool for (a) annealed state and (b) hardened state workpiece of Ni-based alloy.....	33
Figure 1-34 Cutting force (N) versus cutting time (min), (a) F_x and (b) F_y [8]	33
Figure 1-35 Effect of tool wear on cutting force [11]	34
Figure 1-36 Measured flank wear progression with other observed wear modes during the end milling of Inconel 718. $V_c=140$ m/min, $FR=0.15$ mm/tooth, $DoC=0.75$ mm, $a_e=0.2$ mm [11]	34
Figure 1-37 Cutting force of different machining conditions, Aramcharoen and Chuan [33]	35
Figure 1-38 Evolution of the three components and the magnitude of the cutting force (N) as a function of T_{mr} ($^{\circ}C$). $V_c=30$ m/min, $FR=0.10$ mm/tooth, and $DoC=0.2$ mm, Kong et al. [41]	35
Figure 2-1 A Pacific FU.125 milling machine and the arrangement of dynamometer and workpiece	38
Figure 2-2 Illustrations of down-milling experiment: (a) image showing assembly of dynamometer for forces (F_x , F_y and F_z) measurement, 718Plus workpiece, tool holder and insert, coolant nozzle, and (b) schematic of viewing down on the workpiece and tool-insert with various stages of the tool during the pass indicated.....	39

Figure 2-3 (a) A drawing of workpiece blocks, (b) actual workpiece with different block viewing.....	40
Figure 2-3 Continued	41
Figure 2-4 (a) Photo of an insert mounted on a tool holder and actual images of three faces of a tool insert, (a) rake face, (b) side flank face and (c) bottom flank face. (Regions marked by the pink rectangular are cutting areas and thus the major interest/focus areas to be analysed)	42
Figure 2-5 An illustration of the radius cutting edge between cutting insert and the workpiece	42
Figure 2-6 Example of distance between Vickers indentations	43
Figure 2-7 The dimension of tensile specimens.....	44
Figure 2-8 Plot of engineering stress against engineering strain: (a) annealed sample 1, (b) annealed sample 2, (c) hardened sample 1 and (d) hardened sample 2	44
Figure 2-9 Engineering stress (MPa) versus engineering strain; (a) annealed sample 1 and (b) heat treatment sample 1	45
Figure 2-10 Dynamometer setting (a) dynamometer forces F_x , F_y and F_z direction on the machine setting (b) configuration of dynamometer, charge amplifier and milling machine.....	49
Figure 2-11 An illustration of cutting tool insert mounted on epoxy resin.....	50
Figure 2-12 An illustration of an interrupt milling pass with line drawn indicating sectioned sample was made on the machined surface.....	51
Figure 2-13 Machined surface of 718Plus Ni-based superalloy (a) an illustration a cross section machined surface on a bakelite resin and (b) micrograph of the cross section machined surface.....	51
Figure 2-14 Cutting tool insert position at the SEM sample holder for three different view; (a) side flank face, (b) bottom flank face and (c) rake face	52
Figure 2-14 Continued	53
Figure 2-15 Example of flank wear assessment on SEM images on the side flank face; (a) a new tool insert before milling, (b) higher magnification image in location A, (c) higher location magnification image in location B showing fine WC grains in edge location (cutting	

edge) before milling (d) Tool deteriorated after the fourth milling pass. Tooling condition: uncoated carbide and wet (TC12-1).....	53
Figure 2-15 Continued	54
Figure 2-16 SEM images sequences for every passes; (a) side flank face, (b) bottom flank face and (c) rake face. Tooling condition: uncoated carbide and wet (TC12-1).....	54
Figure 2-16 Continued	55
Figure 3-1 SEM images of insert TC1 side flank face before and after various passes: (a) before milling with edge outlined, designated as zero pass edge outline (ZPEO), (b) after the first pass together with ZPEO, (c) after the second pass with ZPEO and (d) after the third pass (magnification different). Tooling condition: uncoated carbide and dry	57
Figure 3-2 Cutting edge features: (a) higher magnification image in location A of Figure 3-1b, showing 718 BUL material next to WC grains edge, (b) higher magnification image in location marked B in (a) showing fine WC grains in edge location, (c) EDS spectrum with analytical spot * marked in (a) and (d) EDS spectrum with analytical spot + marked in (a)	58
Figure 3-3 Illustration of a cross section of new tool insert (SEM images) and workpiece (drawings) indicating features during milling: (a) low magnification SEM image in and around cutting edge location together with drawings indicating the various features in the surrounding and (b) high magnification SEM image in a cutting edge location displaying fine WC grains bound by Co-binder	59
Figure 3-4 SEM images of insert TC2 side flank face before and after various passes: (a) before milling with edge outlined, designated as zero pass edge outline (ZPEO), (b) after the first pass together with ZPEO, (c) after the second pass together with ZPEO, (d) after the third pass together with ZPEO and (e) A higher magnification of image 3-4d indicating plastic lowering on the tool insert	62
Figure 3-5 SEM images of insert TC2 bottom flank face before and after various passes: (a) before milling with zero pass edge outline (ZPEO), (b) after the first pass together with ZPEO, (c) after the second pass together with ZPEO and (d) after the third pass together with ZPEO. Tooling condition: uncoated carbide and dry.....	63
Figure 3-6 SEM images of insert TC2 rake face before and after various passes: (a) before milling with zero pass edge outline (ZPEO), (b) after the first pass together with ZPEO, (c) after the second pass together with ZPEO and (d) after the third pass together with ZPEO, (d) after the third pass together with ZPEO, Chip flow direction is indicated by arrow in each pass. Tooling condition: uncoated carbide and dry.....	64
Figure 3-7 Higher magnification images showing cracks as pointed to by arrows in cutting edge: (a) at location A of Figure 3-5c and (b) at location B of Figure 3-6c	65

Figure 3-8 SEM images of insert TC3 (TiAlN coated) side flank face after (a) before milling, (b) first pass (c) second passes and (d) third passes. Tooling condition: coated carbide and dry	66
Figure 3-9 SEM images of insert TC4 (TiAlN coated) side flank face after two passes, (a) low magnification and (b) very high magnification in location A in (a). Tooling condition: coated carbide and dry	66
Figure 3-10 Schematic summary of severity of tool deterioration observed in this study ..	69
Figure 4-1 Schematic view looking down on the workpiece and tool-insert with various stages of the tool during the pass indicated.....	72
Figure 4-2 The whole F_x , F_y , F_z and F curves (recorded data) of (a) the first milling pass and (b) the fourth milling pass. Tooling condition: uncoated and coolant (TC7-2)	73
Figure 4-3 F_x , F_y , F_z and F data/curves of the first pass during (a) the initial and within 3 s of milling engagement and (b) a half milling cycle time in early milling stage. Tooling condition: uncoated and coolant (TC7-2)	74
Figure 4-4 Geometrical representation of milling, viewing down: (a) at the start of milling engagement meaning the first cycle of a pass, and (b) during a normal milling cycle that the tool insert cuts the workpiece with a full lateral distance (radial depth of cut), a_e . Distance of FR and thus d_{c-w} are not drawn in proportion.....	75
Figure 4-5 F_x , F_y , F_z and F data/curves of the fourth pass during (a) a 3 s period just before the insert reached the end of the workpiece and (b) a half milling cycle time within a period. Tooling condition: uncoated and coolant (TC7-2).....	76
Figure 4-6 Cutting force (F) data/curves of the first pass during the initial 3s of milling engagement of tool conditions; (a)-(b) uncoated and dry, (c)-(d) coated and dry, (e)-(f) uncoated and coolant and (g)-(h) coated and coolant	78
Figure 4-7 SEM images of side flank faces after the first pass of milling of tool conditions: (a)-(b) uncoated and dry, (c)-(d) coated and dry, (e)-(f) uncoated and coolant and (g)-(h) coated and coolant.....	79
Figure 4-8 Average maximum force values F_{x-e-m} , F_{y-e-m} , F_{z-e-m} and F_{e-m} verses the number of passes for the four tooling conditions, (a) uncoated and dry, (b) coated and dry, (c) uncoated and coolant and (d) coated and coolant.....	82
Figure 4-9 SEM images of coated insert and wet (coolant) conditions (TC8-1): (a) side flank face of the insert after the first pass (coating eroded on edge and workpiece build-up are indicated), (b) left - side flank face, mid - bottom flank face and right - rake face, respectively,	

of the insert after five passes, and (c) left - higher magnification image in location marked C in (b) and right – EDS spectrum with analytical spot + marked in the left image. In the right image of (b), how the side flank face view corresponds in the right image and bottom flank view in the mid image are indicated 83

Figure 4-10 VB_{max} verses the number of passes for the four milling conditions, (a) uncoated and dry, (b) coated and dry, (c) uncoated and coolant and (d) coated and coolant..... 84

Figure 4-11 F_{e-m} values plotted as a function of VB_{max} 85

Figure 4-12 SEM images of (a) from left to right side flank face, bottom flank face and rake face of insert TC7-2 after four passes (the edge outline of the insert before milling has been superimposed), corresponding to point B in 4-11 and (b) higher magnification image in location marked B in (a) and EDS spectrum (on spot +) on the right..... 86

Figure 4-13 SEM images of side flank faces: (a) insert TC7-1 after 4 passes and (b) insert TC5-2 after 5 passes. In each image, the edge outline of the insert before milling has been superimposed 87

Figure 4-14 Schematic illustration of milling with (a) the cutting insert in the initial state before deterioration, (b) the insert having worn and thus the radius of cutting edge having enlarged, $r1 < r2$, and (c) the insert having worn and flank face material having fractured off, $r3 \ll r2$ (Note: $r4$ does not need to be equal to $r2$ and $r1$ of the initial cutting edge is not indicated). The projection of the resultant of total force in working plane, F_a , is indicate in (a) and SEM viewing directions and thus VB are indicated (c) 88

Figure 4-15 Illustration of the deforming zone on the machined cross-section surface 90

Figure 4-16 Micro hardness map on the machined cross-section surface; left images are of new tool image and right image is a deteriorated tool after the fourth pass (a)-(b) annealed workpiece, uncoated and dry (TC9), (c)-(d) annealed workpiece, uncoated and wet (coolant) (TC10)..... 91

Figure 4-16 Continued 92

Figure 4-17 SEM images of uncoated and dry (TC9) after the fourth pass (a) side flank face (b) bottom flank face..... 94

Figure 4-18 F curves (recorded data) of (a) the first milling pass of TC9, (b) the final pass milling pass of TC9, (c) the first milling of TC10 and (d) the final milling pass of TC10.. 94

Figure 4-19 The whole F_x , F_y , F_z and F curves (recorded data) of (a) the first milling pass and (b) the third pass. Tooling condition: uncoated carbide and dry (TC11-1)..... 95

Figure 4-20 F_x , F_y , F_z and F curves of the first pass during (a) the initial within 3s of milling engagement and (b) a half milling cycle time in the early milling stage. Tooling condition: uncoated carbide and dry (TC11-1)	96
Figure 4-21 F_x , F_y , F_z and F curves of the first pass during (a) 3-s period just before the insert reached the end of the workpiece and (b) a half milling cycle time within a period. Tooling condition: uncoated carbide and dry (TC11-1)	97
Figure 4-22 Average maximum force values F_{x-e-m} , F_{y-e-m} , F_{z-e-m} and F_{e-m} versus the number of passes for the two tooling (a) TC11 and (b) TC12	98
Figure 4-23 VB_{max} versus the number of passes for the two milling conditions, TC11 and TC12.....	100
Figure 4-24 SEM images of side flank face; (a) before milling, (b) first milling pass, (c) second milling pass and (d) third milling pass. Tooling condition: TC11-2	100
Figure 4-25 SEM images of third pass; (a) bottom flank face and (b) rake flank face, tooling condition: TC11-2	101
Figure 4-26 SEM images of side flank face; (a) before milling, (b) first milling pass, (c) second milling pass and (d) third milling pass. Tooling condition: TC12-1	101
Figure 4-27 F_{e-m} versus VB_{max} for a feed rate of 0.1 mm/rev conditions.....	102
Figure 5-1 VB_{max} versus the number of passes of milling a hardened workpiece : (a) dry (TC13) and (b) wet (coolant) (TC14).....	104
Figure 5-2 SEM images Tool TC13-1 side flank face before and after various milling passes of a hardened workpiece: (a) before milling with edge outlined, designated as zero pass edge outline (ZPEO), (b) after the first pass together with ZPEO, and (c) after the second pass together with ZPEO.....	105
Figure 5-3 SEM images Tool TC13-1 bottom flank face before and after various milling passes of a hardened workpiece: (a) before milling with edge outlined, designated as zero pass edge outline (ZPEO), (b) after the first pass together with ZPEO, and (c) after the second pass together with ZPEO.....	105
Figure 5-3 Continued	106
Figure 5-4 SEM images Tool TC13-1 rake face before and after various milling passes of a hardened workpiece: (a) before milling with edge outlined, designated as zero pass edge outline (ZPEO), (b) after the first pass together with ZPEO, and (c) after the second pass together with ZPEO.....	106

Figure 5-5 SEM images Tool TC13-2 side flank face before and after various milling passes of a hardened workpiece: (a) before milling with edge outlined, designated as zero pass edge outline (ZPEO), (b) after the first pass together with ZPEO, (c) after the second pass together with ZPEO, (d) after the third pass together with ZPEO, and (e) after the fourth pass together with ZPEO..... 107

Figure 5-6 SEM images Tool TC13-2 of rake face before and after various milling passes of a hardened workpiece: (a) before milling with edge outlined, designated as zero pass edge outline (ZPEO), (b) after the first pass together with ZPEO, (c) after the second pass together with ZPEO, (d) after the third pass together with ZPEO, and (e) after the fourth pass together with ZPEO..... 108

Figure 5-7 SEM images Tool TC14-1 side flank face before and after various milling passes of a hardened workpiece: (a) before milling with edge outlined, designated as zero pass edge outline (ZPEO), (b) after the first pass together with ZPEO, (c) after the second pass together with ZPEO, (d) after the third pass together with ZPEO, and (e) after the fourth pass together with ZPEO..... 110

Figure 5-8 SEM images Tool TC14-1 bottom flank face before and after various milling passes of a hardened workpiece: (a) before milling with edge outlined, designated as zero pass edge outline (ZPEO), (b) after the first pass together with ZPEO, (c) after the second pass together with ZPEO, (d) after the third pass together with ZPEO, and (e) after the fourth pass together with ZPEO..... 111

Figure 5-9 SEM images Tool TC14-2 side flank face before and after various milling passes of a hardened workpiece: (a) before milling with edge outlined, designated as zero pass edge outline (ZPEO), (b) after the first pass together with ZPEO, (c) after the second pass together with ZPEO, (d) after the third pass together with ZPEO, and (e) after the fourth pass together with ZPEO..... 112

Figure 5-10 SEM images of tool TC14-2 in milling a hardened workpiece: (a) higher magnification image in location of Figure 5-9d at location A, showing crack initiation at side flank face view, and (b) higher magnification of 5000X magnification at side flank face 113

Figure 5-11 SEM images Tool TC14-2 rake face before and after various milling passes of a hardened workpiece: (a) before milling with edge outlined, designated as zero pass edge outline (ZPEO), (b) after the first pass together with ZPEO, (c) after the second pass together with ZPEO, (d) after the third pass together with ZPEO, and (e) after the fourth pass together with ZPEO..... 113

Figure 5-11 Continue 114

Figure 5-12 SEM images of tool TC14-2 in milling a hardened workpiece: (a) higher magnification image in location of Figure 5-11d at location point B, showing crack initiation at rake face view, and (b) higher magnification of 5000X magnification at the rake face 114

Figure 5-13 The whole F_x , F_y , F_z and F curves (recorded data) of a hardened workpiece (a) the first milling pass and (b) the fourth milling pass. Tooling condition: uncoated and coolant (TC14-1).....	115
Figure 5-13 Continued	116
Figure 5-14 F_x , F_y , F_z and F data/curves of a hardened workpiece for the first pass during (a) the initial and within 3 s of milling engagement and (b) a half milling cycle time in early milling stage. Tooling condition: uncoated and coolant (TC14-1).....	116
Figure 5-14 Continued	117
Figure 5-15 F_x , F_y , F_z and F data/curves of the first pass during (a) a 3-s period just before the insert reached the end of the workpiece and (b) a half cycle time within a period. Tooling condition: uncoated and coolant (TC14-1)	118
Figure 5-16 Average maximum force values F_{x-e-m} , F_{y-e-m} , F_{z-e-m} and F_{e-m} versus the number of passes four two cooling conditions, (a) TC13-1, (b) TC13-2, (c) TC14-1 and (d) TC14-2	119
Figure 5-17 F_{e-m} values as a function of VB_{max}	121
Figure 5-18 Micro hardness map on the cross section machined surface; (a) a new tool insert after the first pass (left image) and a deteriorated tool insert after the fourth milling pass (right image). Tool condition: uncoated tool and dry (TC15)	122
Figure 5-19 SEM images rake face of a deteriorated tool after the fourth pass of milling hardened workpiece in dry condition (TC15)	122
Figure 5-20 F curves (recorded data) of tool insert (a) a new tool after the first pass (b) .	123
Figure 5-21 (a) Cutting force (F_{e-m}) and (b) flank wear (VB_{max}) values plotted against the number of passes (N_{pass}) for milling experiments conducted using annealed workpiece (TC5 and TC7) and hardened workpiece (TC13 and TC14).....	124
Figure 5-22 F_{e-m} values plotted as a function of VB_{max} for experiments using both annealed and hardened workpieces	125
Figure 5-23 (a) Cutting force (F_{e-m}) and (b) flank wear (VB_{max}) values plotted against the number of passes (N_{pass}) for various tool conditions using annealed and heat treatment workpieces.....	126

LIST OF TABLES

Table 2-1	Composition specification of 718Plus (wt%).	40
Table 2-2	Heat treatment of 718 Plus.....	41
Table 2-3	Summary of milling condition of 718Plus experimental conditions.	47

NOMENCLATURE

ω - Spindle Speed

$\tau_{Cutting}$ - Shear Stress

θ_e - Effective Rake Angle

a_e - Radial Depth of Cut

BUE – Build-Up Edge

BUL - Build-Up Layer

Co - Cobalt

CrN - Chromium Nitride

d_{c-w} / h - Thickness of Cut

DoC - Depth of Cut

EDS - Energy Dispersive Spectrometry

f or FR - Feed Rate

F or $F_{Cutting}$ - Cutting Force

F_a - working plane

$F_{Cutting-R}$ - Cutting Edge Action Force

F_f - Friction Force

F_R - Resultant Force

F_x - Force in x -direction

F_y - Force in y -direction

F_z - Force in z -direction

F_{x-m} - The maximum F_x started to decrease when the end of the pass was reached

F_{y-m} - The maximum F_y started to decrease when the end of the pass was reached

F_{z-m} - The maximum F_z started to decrease when the end of the pass was reached

F_m - The maximum F started to decrease when the end of the pass was reached

F_{x-e-m} - The maximum F_x of 3 s period just before the insert reached the end of workpiece

F_{y-e-m} - The maximum F_y of 3 s period just before the insert reached the end of workpiece

F_{z-e-m} - The maximum F_z of 3 s period just before the insert reached the end of workpiece

F_{e-m} - The maximum F of 3 s period just before the insert reached the end of workpiece

HRC - Hardness Rockwell C

HV - Hardness Vickers

ISO - International Organisation for Standardisation

MAZ - Milling Affected Zone

MQL - Minimum Quantity Lubrication

Ni - Nickel

N_{pass} - Number of Tool Passes

PCD - Polycrystalline Diamond

PVD - Physical Vapour Deposition

r_e - Cutting Edge Radius

r_{e-eff} - Effective Radius of the Cutting Edge

SEM – Scanning Electron Microscope

t_0 - Original Cutting Edge Geometry

TC -Tool Condition

TDA - Tool Deterioration Area

t_i - Original Cutting Edge Geometry after the wearing process

TiAlN - Titanium Aluminium Nitride

TiC - Titanium Carbide

TiN - Titanium Nitride

v - Forward Speed

V - Tool Forward Speed

VB - Flank Wear

$VB1$ - Uniform Flank Wear

$VB2$ - Non-Uniform Wear

$VB3$ - Localised Flank Wear

VB_{max} - Maximum Flank Wear (localised)

V_c – Cutting Speed

VTW - Volume Tool Wear

V_{wear} - Volume of Wear

WC - Tungsten Carbide

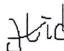
WC-Co - Cemented Tungsten Carbide

ZPEO - Zero Pass Edge Outline

ATTESTATION OF AUTHORSHIP

I hereby declare that this submission is my own work and that, to the best of my knowledge and belief, it contains no material previously published or written by another person (except where explicitly defined in the acknowledgements), nor material which to a substantial extent has been submitted for the award of any other degree or diploma of a university or other institution of higher learning.

Auckland

Signature  _____

References

- [1] V. P. Astakhov, *Machinability of Advanced Materials*, First Edit. ISTE Ltd and John Wiley & Sons, INC, 2014.
- [2] S. Pervaiz, A. Rashid, I. Deiab, and M. Nicolescu, "Influence of Tool Materials on Machinability of Titanium- and Nickel-Based Alloys: A Review," *Mater. Manuf. Process.*, vol. 29, no. 3, pp. 219–252, 2014.
- [3] Y. S. Liao, H. M. Lin, and J. H. Wang, "Behaviors of end milling Inconel 718 superalloy by cemented carbide tools," *J. Mater. Process. Technol.*, vol. 201, no. 1–3, pp. 460–465, 2008.
- [4] X. Q. Chen and H. Z. Li, "Development of a tool wear observer model for online tool condition monitoring and control in machining nickel-based alloys," *Int. J. Adv. Manuf. Technol.*, vol. 45, no. 7–8, pp. 786–800, 2009.
- [5] K. Kadirgama, K. A. Abou-El-Hossein, M. M. Noor, K. V. Sharma, and B. Mohammad, "Tool life and wear mechanism when machining Hastelloy C-22HS," *Wear*, vol. 270, no. 3–4, pp. 258–268, 2011.
- [6] A. Devillez, G. Le Coz, S. Dominiak, and D. Dudzinski, "Dry machining of Inconel 718, workpiece surface integrity," *J. Mater. Process. Technol.*, vol. 211, no. 10, pp. 1590–1598, 2011.
- [7] S. Olovsjö and L. Nyborg, "Influence of microstructure on wear behaviour of uncoated WC tools in turning of Alloy 718 and Waspaloy," *Wear*, vol. 282–283, pp. 12–21, 2012.
- [8] S. Zhang, J. F. Li, and Y. W. Wang, "Tool life and cutting forces in end milling Inconel 718 under dry and minimum quantity cooling lubrication cutting conditions," *J. Clean. Prod.*, vol. 32, pp. 81–87, 2012.
- [9] irfan Uzun, K. Aslantas, and F. Bedir, "An experimental investigation of the effect of coating material on tool wear in micro milling of Inconel 718 super alloy," *Wear*, vol. 300, no. 1–2, pp. 8–19, 2013.
- [10] M. Imran, P. T. Mativenga, A. Gholinia, and P. J. Withers, "Comparison of tool wear mechanisms and surface integrity for dry and wet micro-drilling of nickel-base superalloys," *Int. J. Mach. Tools Manuf.*, vol. 76, pp. 49–60, 2014.
- [11] M. S. Kasim, C. H. Che Haron, J. A. Ghani, M. A. Sulaiman, and M. Z. A. Yazid,

- “Wear mechanism and notch wear location prediction model in ball nose end milling of Inconel 718,” *Wear*, vol. 302, no. 1–2, pp. 1171–1179, 2013.
- [12] D. Zhu, X. Zhang, and H. Ding, “Tool wear characteristics in machining of nickel-based superalloys,” *Int. J. Mach. Tools Manuf.*, vol. 64, pp. 60–77, 2013.
- [13] S. Chinchani and S. K. Choudhury, “Machining of hardened steel - Experimental investigations, performance modeling and cooling techniques: A review,” *Int. J. Mach. Tools Manuf.*, vol. 89, pp. 95–109, 2015.
- [14] L. N. L. De Lacalle, A. Lamikiz, J. F. De Larrinoa, and I. Azkona, “Advanced Cutting Tools,” *Machining of Hard Materials*, Springer-Verlag, London, 2011, pp.33-86.
- [15] ISO 8688-2, International Organisation for Standardization, Geneva, 1989.
- [16] H. G. Prengel, W. R. Pfouts, and A. T. Santhanam, “State of the art in hard coatings for carbide cutting tools,” *Surf. Coatings Technol.*, vol. 102, no. 3, pp. 183–190, 1998.
- [17] A. Jawaid, S. Koksai, and S. Sharif, “Cutting performance and wear characteristics of PVD coated and uncoated carbide tools in face milling Inconel 718 aerospace alloy,” *J. Mater. Process. Technol.*, vol. 116, no. 1, pp. 2–9, 2001.
- [18] M. Kuttalamadom, “Prediction of the Wear & Evolution of Cutting Tools in a Carbide / Ti-6Al-4V Machining Tribosystem by Volumetric Tool Wear Characterization & Modeling,” p. 258, 2012.
- [19] M.-D. Jimenez, A.-E. Bermudez, “Friction and wear,” in *Industrial Lubrication and Tribology*, vol. 36, no. 5, J. P. Davim, Ed. Woodhead Publishing Limited, 1984, pp. 168–169.
- [20] M. C. Shaw, *Second Edition*, Second. Oxford series on Advanced manufacturing, , pp. 170, 2005.
- [21] J. a. Charles, *Selection and Use of Engineering Materials*, Third. Butterworth Heinemann, 1997.
- [22] H. Z. Li, H. Zeng, and X. Q. Chen, “An experimental study of tool wear and cutting force variation in the end milling of Inconel 718 with coated carbide inserts,” *J. Mater. Process. Technol.*, vol. 180, no. 1–3, pp. 296–304, 2006.
- [23] W. Akhtar, J. Sun, P. Sun, W. Chen, and Z. Saleem, “Tool wear mechanisms in

- the machining of Nickel based super-alloys: A review,” *Front. Mech. Eng.*, vol. 9, no. 2, pp. 106–119, 2014.
- [24] E. O. Ezugwu, Z. M. Wang, and A. R. Machado, “The machinability of nickel-based alloys: a review,” *J. Mater. Process. Technol.*, vol. 86, no. 1, pp. 1–16, 1999.
 - [25] E. O. Ezugwu, J. Bonney, and Y. Yamane, “An overview of the machinability of aeroengine alloys,” *J. Mater. Process. Technol.*, vol. 134, no. 2, pp. 233–253, 2003.
 - [26] Y. Huang and S. Y. Liang, “Modeling of CBN Tool Flank Wear Progression in Finish Hard Turning,” *J. Manuf. Sci. Eng.*, vol. 126, no. 1, p. 98, 2004.
 - [27] A. Shokrani, V. Dhokia, S. T. Newman, and R. Imani-Asrai, “An initial study of the effect of using liquid nitrogen coolant on the surface roughness of inconel 718 nickel-based alloy in CNC milling,” *Procedia CIRP*, vol. 3, no. 1, pp. 121–125, 2012.
 - [28] D. Dudzinski, A. Devillez, A. Moufki, D. Larrouquère, V. Zerrouki, and J. Vigneau, “A review of developments towards dry and high speed machining of Inconel 718 alloy,” *Int. J. Mach. Tools Manuf.*, vol. 44, no. 4, pp. 439–456, 2004.
 - [29] T. Obikawa, Y. Kamata, Y. Asano, K. Nakayama, and A. W. Otieno, “Micro-liter lubrication machining of Inconel 718,” *Int. J. Mach. Tools Manuf.*, vol. 48, no. 15, pp. 1605–1612, 2008.
 - [30] Y. Kamata and T. Obikawa, “High speed MQL finish-turning of Inconel 718 with different coated tools,” *J. Mater. Process. Technol.*, vol. 192–193, pp. 281–286, 2007.
 - [31] F. Pusavec, H. Hamdi, J. Kopac, and I. S. Jawahir, “Surface integrity in cryogenic machining of nickel based alloy—Inconel 718,” *J. Mater. Process. Technol.*, vol. 211, no. 4, pp. 773–783, 2011.
 - [32] D. Fernández, V. García Navas, A. Sandá, and I. Bengoetxea, “Comparison of machining inconel 718 with conventional and sustainable coolant,” *MM Sci. J.*, no. December 2014, pp. 506–510, 2014.
 - [33] A. Aramcharoen and S. K. Chuan, “An experimental investigation on cryogenic milling of inconel 718 and its sustainability assessment,” *Procedia CIRP*, vol. 14, pp. 529–534, 2014.
 - [34] Y. Kaynak, H. E. Karaca, R. D. Noebe, and I. S. Jawahir, “Tool-wear analysis in

- cryogenic machining of NiTi shape memory alloys: A comparison of tool-wear performance with dry and MQL machining,” *Wear*, vol. 306, no. 1–2, pp. 51–63, 2013.
- [35] J. A. Ghani, I. A. Choudhury, and H. H. Masjuki, “Wear mechanism of TiN coated carbide and uncoated cermets tools at high cutting speed applications,” *J. Mater. Process. Technol.*, vol. 153–154, no. 1–3, pp. 1067–1073, 2004.
 - [36] A. Sharman, R. C. Dewes, and D. K. Aspinwall, “Tool life when high speed ball nose end milling Inconel 718™,” *J. Mater. Process. Technol.*, vol. 118, no. 1–3, pp. 29–35, Dec. 2001.
 - [37] H. G. Prengel, P. C. Jindal, K. H. Wendt, A. T. Santhanam, P. L. Hegde, and R. M. Penich, “A new class of high performance PVD coatings for carbide cutting tools,” *Surf. Coatings Technol.*, vol. 139, no. 1, pp. 25–34, 2001.
 - [38] L. Li, N. He, M. Wang, and Z. G. Wang, “High speed cutting of Inconel 718 with coated carbide and ceramic inserts,” *J. Mater. Process. Technol.*, vol. 129, no. 1–3, pp. 127–130, 2002.
 - [39] C. Ducros, V. Benevent, and F. Sanchette, “Deposition, characterization and machining performance of multilayer PVD coatings on cemented carbide cutting tools,” *Surf. Coatings Technol.*, vol. 163–164, pp. 681–688, 2003.
 - [40] M. Sortino, S. Belfio, G. Totis, E. Kuljanic, and G. Fadelli, “Innovative tool coatings for increasing tool life in milling Nickel-coated Nickel-Silver alloy,” *Energy Procedia*, vol. 100, no. C, pp. 946–952, 2015.
 - [41] X. Kong, L. Yang, H. Zhang, K. Zhou, and Y. Wang, “Cutting performance and coated tool wear mechanisms in laser-assisted milling K24 nickel-based superalloy,” *Int. J. Adv. Manuf. Technol.*, vol. 77, no. 9–12, pp. 2151–2163, 2015.
 - [42] B. Kaya, C. Oysu, and H. M. Ertunc, “Force-torque based on-line tool wear estimation system for CNC milling of Inconel 718 using neural networks,” *Adv. Eng. Softw.*, vol. 42, no. 3, pp. 76–84, 2011.
 - [43] M. Nouri, B. K. Fussell, B. L. Ziniti, and E. Linder, “Real-time tool wear monitoring in milling using a cutting condition independent method,” *Int. J. Mach. Tools Manuf.*, vol. 89, pp. 1–13, 2015.
 - [44] S. Chinchankar and S. K. Choudhury, “Cutting force modeling considering tool wear effect during turning of hardened AISI 4340 alloy steel using multi-layer

- TiCN/Al₂O₃/TiN-coated carbide tools,” *Int. J. Adv. Manuf. Technol.*, vol. 83, no. 9–12, pp. 1749–1762, 2016.
- [45] C. H. Lauro, L. C. Brandão, D. Baldo, R. A. Reis, and J. P. Davim, “Monitoring and processing signal applied in machining processes - A review,” *Meas. J. Int. Meas. Confed.*, vol. 58, pp. 73–86, 2014.
- [46] L. Whitmore *et al.*, “The microstructure of heat-treated nickel-based superalloy 718Plus,” *Mater. Sci. Eng. A*, vol. 610, pp. 39–45, 2014.
- [47] T. D. Sheet, “ATI 718Plus ® Alloy 1,” vol. 1, pp. 1–5, Allegheny Technologies Incorporated, 2013.
- [48] V. P. Astakhov, “The assessment of cutting tool wear,” *Int. J. Mach. Tools Manuf.*, vol. 44, no. 6, pp. 637–647, 2004.
- [49] M. Kuttolamadom, P. Mehta, L. Mears, and T. Kurfess, “Correlation of the Volumetric Tool Wear Rate of Carbide Milling Inserts With the Material Removal Rate of Ti–6Al–4V,” *J. Manuf. Sci. Eng.*, vol. 137, no. 2, p. 21021, 2015.
- [50] M. A. Kuttolamadom and M. L. Mears, “Msec2011-50278 on the Volumetric Assessment of Tool Wear in Machining,” pp. 1–10, 2011.
- [51] Chetan, B. C. Behera, S. Ghosh, and P. V. Rao, “Wear behavior of PVD TiN coated carbide inserts during machining of Nimonic 90 and Ti6Al4V superalloys under dry and MQL conditions,” *Ceram. Int.*, vol. 42, no. 13, pp. 14873–14885, 2016.
- [52] N. H. Razak, Z. W. Chen, and T. Pasang, “Modes of tool deterioration during milling of 718Plus superalloy using cemented tungsten carbide tools,” *Wear*, vol. 316, pp. 92–100, 2014.
- [53] A. Introduction, M. F. Ashby, and D. R. H. Jones, *Engineering Materials 2*. 1986.
- [54] T. Kitagawa, A. Kubo, and K. Maekawa, “Temperature and wear of cutting tools in high-speed machining of Inconel 718 and Ti–6Al–6V–2Sn,” *Wear*, vol. 202, no. 2, pp. 142–148, 1997.
- [55] L. Zhang, X. Qu, X. He, D. Rafi-Ud, M. Qin, and H. Zhu, “Hot deformation behavior of Co-base ODS alloys,” *J. Alloys Compd.*, vol. 512, no. 1, pp. 39–46, 2012.
- [56] R & D ISCAR Ltd., “of ISCAR Grades Substrate - IC 28 Grade - IC 928 Typical Layers,” *Gen. Inf. ISCAR Grades*, p. 9970165, 2013.

- [57] X. Ren and Z. Liu, "Influence of cutting parameters on work hardening behavior of surface layer during turning superalloy Inconel 718," *Int. J. Adv. Manuf. Technol.*, pp. 2319–2327, 2016.